Vol. 75: 33–51, 2018
https://doi.org/10.3354/cr01504

CLIMATE RESEARCH
Clim Res

Published online March 21

Regional climate change after the commissioning of the Three Gorges Dam: a case study for the middle reaches of the Yangtze River

Feifan Ge[1], Kebiao Mao[1,2,3,*], Yuelin Jiang[1], Lei Wang[4], Tongren Xu[3], Chunyu Gao[2], Zhiyuan Zuo[2]

[1]School of Resources and Environment, Anhui Agricultural University, Hefei 230036, PR China

[2]National Hulunber Grassland Ecosystem Observation and Research Station, Institute of Agricultural Resources and Regional Planning, Chinese Academy of Agricultural Sciences, Beijing 100081, PR China

[3]State Key Laboratory of Remote Sensing Science, Institute of remote sensing and Digital Earth Research, Chines Academy of Science and Beijing Normal University, Beijing 100086, PR China

[4]State Key Laboratory of Numerical Modeling for Atmospheric Sciences and Geophysical Fluid Dynamics, Institute of Atmospheric Physics, Chinese Academy of Sciences, Beijing 100086, PR China

ABSTRACT: The Three Gorges Dam (TGD) has caused hydrological regime changes in the region downstream of the dam. Based on meteorological station data, this study focused on regional climate changes by evaluating several climatic factors in the middle reaches of the Yangtze River and investigated the mutation time of the number of high and low temperature days using the Mann-Kendall (MK) test. We also examined the vegetation response to regional climate change and variations induced by this in the land surface temperature, utilizing the enhanced vegetation index (EVI) and land surface temperature (LST) images, respectively. The study defined 3 stages related to the construction and commissioning time of the TGD. The regional climate before and after the commissioning of the TGD displayed opposite trends in temperatures, including daily mean, maximum and minimum temperatures. Temperatures tended to decrease in the northern portion of the study area, and increase in the southern portion of the study area. MK test results indicated that the mutation times of the number of high and low temperature days occurred around the time that the dam began commissioning to regulate the water flow. Precipitation decreased in the study area, particularly in the Dongting Lake region and its surrounding areas. Vegetation coverage generally increased in most of the southern study area in response to the change in climate. Moreover, the LST trends in the different regions were affected by the changes in vegetation.

KEY WORDS: High and low temperature days · Spatial variability · Precipitation · Vegetation

1. INTRODUCTION

The Yangtze River flows through south-central China and originates from the Qinghai Tibetan Plateau. The river flows eastward for more than 6300 km and drains an area of >1.94×10^6 km^2 before finally discharging into the East China Sea (Liu et al. 2007). As one of the major rivers of the world, the Yangtze River plays a critical role in the global water cycle, sediment cycle, energy balance, climate change and ecological development, and it exhibits seasonal variability in its water levels and area because of monsoon-driven precipitation (Li et al. 2011, Zeng et al. 2013). Thus, high water levels and an increased area are observed in the wet season from May to October and low water levels and a reduced area are ob-

*Corresponding author: maokebiao@126.com

served in the dry season from November to the following April (Li et al. 2011).

The Three Gorges Dam (TGD) is the largest hydroelectric project in the world. It is located 44 km upstream of Yichang station, which is the control point of the upper Yangtze River basin. Many lakes are located downstream of the TGD. Among these, Poyang Lake (28° 11′ to 29° 51′ N, 115° 31′ to 117° 06′ E) and Dongting Lake (28° 30′ to 29° 38′ N, 112° 18′ to 113° 15′ E) are the 2 largest freshwater lakes in China (Feng et al. 2013, Q Zhang et al. 2014). Both lakes receive water from tributaries as well as from the Yangtze River, and both empty into the Yangtze River (Du et al. 2011, Wu et al. 2013).

The TGD project began in 1994, and commissioning started in 2003; however, limited regulation capacity was provided during the initial stage between 2003 and 2005. A transitional stage began in 2006, when the water level of the dam reservoir was raised to 156 m; this stage was completed in 2009 (Deng et al. 2016). During normal operations, the water level fluctuates seasonally between 145 and 175 m in response to water release and storage, and the storage capacity varies between 17.2 and 39.3 km^3 (Yang et al. 2014). Previous studies have shown that the damming of rivers has impacted natural wetlands around the world (Chai et al. 2009, Wu et al. 2013), and that dams inevitably change river flow regimes (Wu et al. 2013). Although the Yangtze has proven to be a hydrologically resilient river (Chen et al. 2014), changes have occurred in the monthly and seasonal flows that are not detectable at the annual scale (J Chen et al. 2016). The TGD has been in operation since 2003, and it has affected the discharge and water levels of the Yangtze River and substantially altered the downstream flow regime. The significance of these effects varies between seasons and locations along the river, and the seasonal variations largely follow the seasonal impoundment of the TGD and its release of water. Moreover, the magnitude of the variation is dependent on the impoundment, release rate and seasonal flow of the river which is determined by the regional climate (J Chen et al. 2016, Y Wang et al. 2016). These variations have caused considerable upward trends in the outflow of lakes to the river, and most lakes in the Yangtze River basin have experienced significant downward trends in water storage during this period, with the total water storage of the lakes decreasing by 14 million m^3 mo^{-1} (Guo et al. 2012, Cai et al. 2016). Dongting Lake and Poyang Lake have exhibited serious reductions in water area since 2003, and the wetland area has increased; moreover, the season with low water levels in the lakes is occurring sooner than before the dam was constructed, and the duration of low water levels has increased (Yuan et al. 2015, Mei et al. 2016).

Many major rivers worldwide are regulated by dams, which induce alterations in flow, sediment, and water temperature regimes (Pegg et al. 2003, Nilsson et al. 2005, Syvitski et al. 2005, Yang et al. 2008), Woldemichael et al. (2014) indicated that dam-triggered land use and land cover can change regional temperature and precipitation patterns. Although the TGD was built to realize flood control, navigation and hydropower generation, the project has created environmental problems that have attracted the attention of environmental activists, researchers and communities around the world. Studies have evaluated the effects of the TGD on the hydrology (Nakayama & Shankman 2013a, Jiang et al. 2014, Liu et al. 2016, Y Wang et al. 2016), sedimentation (S Yang et al. 2002, 2007, 2011, Z Yang et al. 2006, Xu & Milliman 2009, Li et al. 2011, Dai et al. 2016, Du et al. 2016, Zhou et al. 2016) and ecosystem (Müller et al. 2008, Ye et al. 2012, Li et al. 2013, Nakayama & Shankman 2013b, S Chen et al. 2016, Li et al. 2016, Ma et al. 2016, Y Wang et al. 2016) in the region. The effect of the TGD on regional climate has also been analyzed in previous studies. For instance, Yao et al. (2013) noted that the Three Gorges reservoir increased the air temperature in winter and decreased the air temperature in summer. Moreover, after the impoundment, most parts of the Three Gorges Reservoir area reported a temperature rise (Jiao et al. 2013, Yao et al. 2013), with the numbers of high and low temperature days in the reservoir area experiencing a 32 percent increase and 21 percent decrease, respectively (Jiao et al. 2013). Precipitation declined in most of the reservoir area after the impoundment (Jiao et al. 2013), and has been significantly reduced in the Xiangxi River watershed in September (Han et al. 2014). Wu et al. (2006) suggested that the climatic effect of the TGD is on a regional scale (100 km) rather than a local scale (10 km), and that the construction of the TGD has increased precipitation in the region between the Daba and Qinling mountains. However, most studies have focused on the reservoir area, whereas climate change in the regions downstream of the TGD is rarely reported. Previous research has shown that climate change affects the land surface (Bossa et al. 2014, Jiang & Zhang 2015, Stagl & Hattermann 2015, Congjian et al. 2016, Fay et al. 2016, S Kim et al. 2016, Naz et al. 2016, Qin et al. 2016, Toure et al. 2016, G Wang et al. 2016), and that land surface alterations can also impact regional climate (Gao et al. 2014, Cao et al. 2015, Chacón et al. 2016, Halder et al. 2016, H Kim et al. 2016, Sylla et al. 2016). The TGD has altered the hydrological regime in the middle reaches of the Yangtze River (Y Wang et al. 2016), but the effect is diminished in the lower reaches of the Yangtze River (Guo et al. 2012). Thus, an interesting question arises: How have changes in the hydrological regime and underlying surface affected the other climatological variables in the middle reaches of the Yangtze River downstream of the TGD? A detailed analysis is needed to better inform the TGD operations and ecological management of the Yangtze River. In this study, we analyzed changes in several climatological variables (including daily mean, maximum, minimum surface temperatures, daily accumulated precipitation and daily diurnal temperature range) in the middle reaches of the Yangtze River based on observations, assessed the mutation time of the number of high and low temperature days via the Mann-Kendall (MK) test, and used remote sensing data to investigate changes in the vegetation growth status. Our study aimed to determine the regional climate changes caused by anthropogenic hydrological regime changes and to provide a reference for further research.

2. STUDY AREA AND DATA RESOURCE

Because the impacts of the TGD on river discharge rapidly weaken with distance from the TGD (Guo et al. 2012), we set the study area in the middle reaches of the Yangtze River, which encompasses Hubei, Hunan and Jiangxi provinces (24° 27′ to 33° 18′ N, 108° 20′ to 118° 31′ E) (Fig. 1).

This study used a meteorological data set that includes the daily surface air mean, maximum and minimum temperatures, and daily accumulated pre-

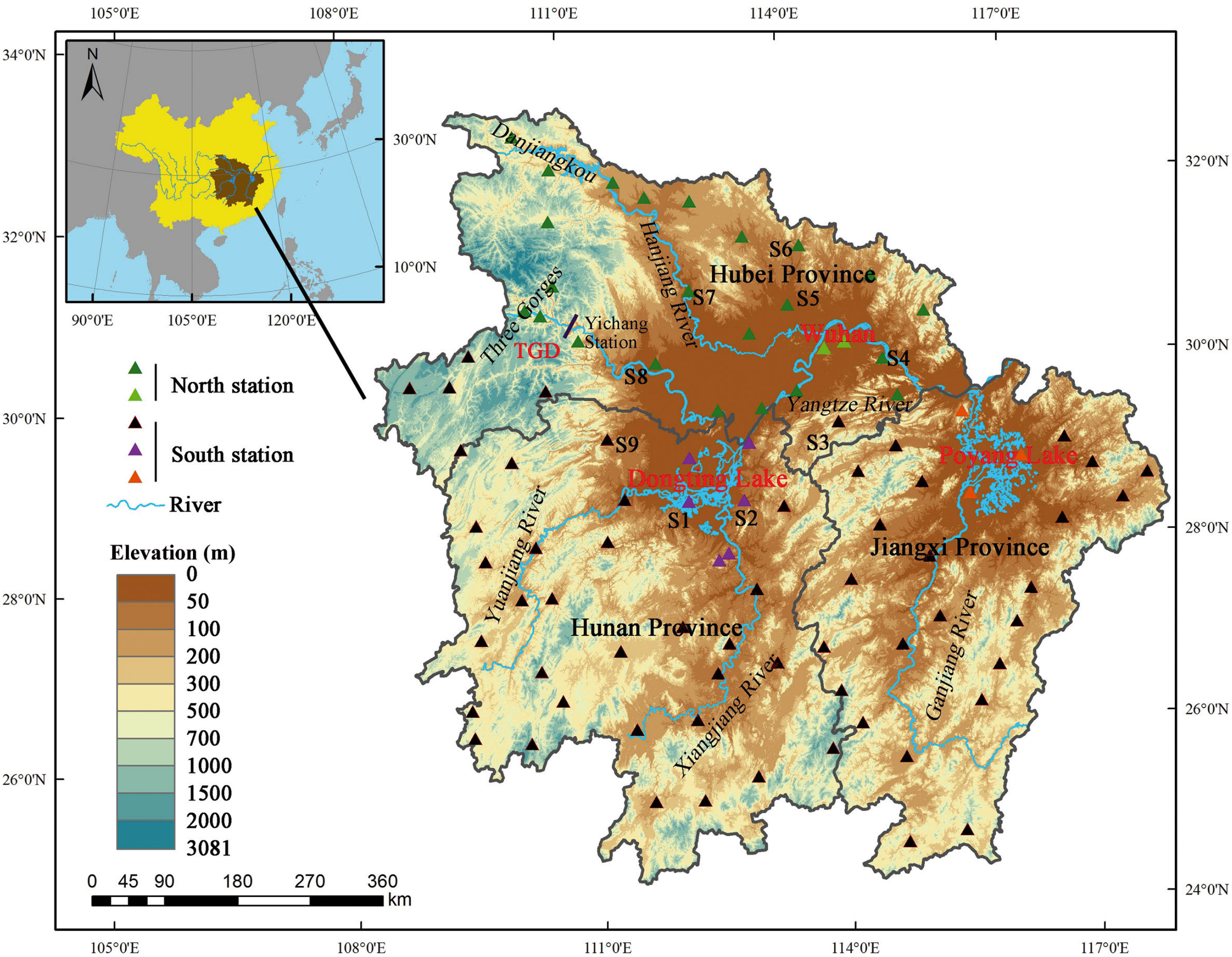

Fig. 1. Study area and meteorological stations. Grey lines: province boundaries; stations are divided into south and north by the Yangtze River

cipitation obtained from the National Meteorological Information Center of the China Meteorological Administration (Li et al. 2017) (http://data.cma.cn). The data set includes data from 824 meteorological stations covering mainland China (16° 32′ to 53° 29′ N, 75° 11′ to 132° 58′ E), most of which were established in the 1950s. The data have been quality controlled (including gross error limit checks, internal and time consistency checks, space and time consistency checks, manual verification and correction) by the National Meteorological Information Center of the China Meteorological Administration. Based on the completeness of the data, times series covering the period 1971–2015 were ultimately selected from 90 of the 92 stations in the study area, and the limited amount of missing data was corrected by the average value of 4 nearby stations. The remote sensing data utilized in this study are the Moderate Resolution Imaging Spectrometer (MODIS) Terra Vegetation Index Monthly L3 Global 1 km product, MOD13A3, and the Land Surface Temperature (LST) 8-Day L3 Global 1 km product, MOD11A2, obtained during 2001–2015 by the National Aeronautics and Space Administration (NASA). The MODIS vegetation index products are designed to provide consistent spatial and temporal comparisons of global vegetation conditions that can be used to monitor photosynthetic activity (Justice et al. 1998). Among the 2 MODIS vegetation indexes, the normalized difference vegetation index (NDVI) and the enhanced vegetation index (EVI), the NDVI is sensitive to chlorophyll contents, whereas the EVI is more responsive to canopy structural variations, including the leaf area index, canopy type, plant physiognomy and canopy architecture (Gao et al. 2000). The NDVI displays asymptotic saturation in high biomass regions, whereas the EVI remains sensitive to canopy variations. In addition, the EVI has a stronger linear relationship with gross primary production than the NDVI (Huete et al. 2002, Xiao et al. 2004). In our study, we focused on the analysis of the EVI and LST to analyze the dynamics of the predominantly lush vegetation and land surface temperature in the middle reaches of the Yangtze River.

3. METHODS

3.1. Study period

Based on the construction periods of the TGD described in Section 1, we divided the study period into 3 stages: the pre-construction stage (stage 1) between 1971 and 1994, the construction stage (stage 2) between 1995 and 2006 and the commissioning stage (stage 3) between 2007 and 2015 when the TGD began to affect the downstream river flow. The meteorological data cover all 3 stages, but the MODIS data only cover parts of stage 2 and stage 3.

3.2. Climatic factors

We investigated differences in climatic factors between 2 stages (from stage 1 to stage 2 and from stage 2 to stage 3) in summer (June to August) and winter (December to February), respectively. We used the inverse distance weight interpolation method to obtain the results on the surface. The variable names are consistent throughout all formulas (Eqs. 1–24).

3.2.1. Temperature

The daily mean temperature in both summer and winter, the daily maximum temperature in summer and the daily minimum temperature in winter were examined to investigate seasonal changes from stage 1 to stage 2 and from stage 2 to stage 3. In this study, global warming was considered by using a total of 518 meteorological stations from a broader area (yellow area in Fig. 1; approximately 6 times larger than the study area and without high altitude and extreme terrain areas), which encompassed the 90 stations of our study area, to eliminate the interference of global warming (see Sections 4.1 and 4.2). The temperature changes of a single station from one stage to the next can be expressed as follows:

$$\Delta_{x_2x_1}\overline{T}_s(n) = \left(\overline{T}_s^{x_2}(n) - \overline{T}_s^{x_1}(n)\right) - \left(\overline{Tf}_s^{x_2}(n) - \overline{Tf}_s^{x_1}(n)\right) \quad (1)$$

$$\Delta_{x_2x_1}\overline{T}_w(n) = \left(\overline{T}_w^{x_2}(n) - \overline{T}_w^{x_1}(n)\right) - \left(\overline{Tf}_w^{x_2}(n) - \overline{Tf}_w^{x_1}(n)\right) \quad (2)$$

$$\Delta_{x_2x_1}\overline{T}_{s\max}(n) = \left(\overline{T}_{s\max}^{x_2}(n) - \overline{T}_{s\max}^{x_1}(n)\right) - \left(\overline{Tf}_{s\max}^{x_2}(n) - \overline{Tf}_{s\max}^{x_1}(n)\right) \quad (3)$$

$$\Delta_{x_2x_1}\overline{T}_{w\min}(n) = \left(\overline{T}_{w\min}^{x_2}(n) - \overline{T}_{w\min}^{x_1}(n)\right) - \left(\overline{Tf}_{w\min}^{x_2}(n) - \overline{Tf}_{w\min}^{x_1}(n)\right) \quad (4)$$

where $\Delta_{x_2x_1}\overline{T}_s(n)$, $\Delta_{x_2x_1}\overline{T}_w(n)$, $\Delta_{x_2x_1}\overline{T}_{s\max}(n)$ and $\Delta_{x_2x_1}\overline{T}_{w\min}(n)$ represent the changes in the daily mean temperatures in summer, the daily mean temperatures in winter (Section 4.1), the daily maximum temperatures in summer and the daily minimum temperatures in winter (Section 4.2) at station n from stage x_1 to x_2, respectively, and $\overline{T}_s^{x_i}(n)$, $\overline{T}_{s\max}^{x_i}(n)$, $\overline{T}_w^{x_i}(n)$ and

$\overline{T}^{x_i}_{w\min}(n)$ represent the mean summer daily mean temperatures, the mean summer daily maximum temperatures, the mean winter daily mean temperatures and the mean winter daily minimum temperatures at station n in stage $x_i(i = 1, 2, 3)$, respectively. $Tf^{x_i}_s(n)$, $Tf^{x_i}_{s\max}(n)$, $Tf^{x_i}_w(n)$ and $Tf^{x_i}_{w\min}(n)$ denote the respective temperatures of the wider area in stage x_i. The above variables are expressed as follows:

$$\overline{T}^{x_i}_s(n) = \frac{\sum_{i=t_1}^{t_2}\left(\frac{1}{k_i}\sum_{j=1}^{k_i} T^{ij}_s(n)\right)}{t_2 - t_1 + 1} \tag{5}$$

$$\overline{T}^{x_i}_w(n) = \frac{\sum_{i=t_1}^{t_2}\left(\frac{1}{k_i}\sum_{j=1}^{k_i} T^{ij}_w(n)\right)}{t_2 - t_1 + 1} \tag{6}$$

$$\overline{T}^{x_i}_{s\max}(n) = \frac{\sum_{i=t_1}^{t_2}\left(\frac{1}{k_i}\sum_{j=1}^{k_i} T^{ij}_{s\max}(n)\right)}{t_2 - t_1 + 1} \tag{7}$$

$$\overline{T}^{x_i}_{w\min}(n) = \frac{\sum_{i=t_1}^{t_2}\left(\frac{1}{k_i}\sum_{j=1}^{k_i} T^{ij}_{w\min}(n)\right)}{t_2 - t_1 + 1} \tag{8}$$

$$\overline{Tf}^{x_i}_s(n) = \frac{1}{N}\sum_{n=1}^{N}\left(\frac{1}{t_2 - t_1 + 1}\sum_{i=t_1}^{t_2}\left(\frac{1}{k_i}\sum_{j=1}^{k_i} T^{ij}_s(n)\right)\right) \tag{9}$$

$$\overline{Tf}^{x_i}_w(n) = \frac{1}{N}\sum_{n=1}^{N}\left(\frac{1}{t_2 - t_1 + 1}\sum_{i=t_1}^{t_2}\left(\frac{1}{k_i}\sum_{j=1}^{k_i} T^{ij}_w(n)\right)\right) \tag{10}$$

$$\overline{Tf}^{x_i}_{s\max}(n) = \frac{1}{N}\sum_{n=1}^{N}\left(\frac{1}{t_2 - t_1 + 1}\sum_{i=t_1}^{t_2}\left(\frac{1}{k_i}\sum_{j=1}^{k_i} T^{ij}_{s\max}(n)\right)\right) \tag{11}$$

$$\overline{Tf}^{x_i}_{w\min}(n) = \frac{1}{N}\sum_{n=1}^{N}\left(\frac{1}{t_2 - t_1 + 1}\sum_{i=t_1}^{t_2}\left(\frac{1}{k_i}\sum_{j=1}^{k_i} T^{ij}_{w\min}(n)\right)\right) \tag{12}$$

where $T^{ij}_s(n)$, $T^{ij}_{s\max}(n)$, $T^{ij}_w(n)$ and $T^{ij}_{w\min}(n)$ are the summer daily mean temperatures, the summer daily maximum temperatures, the winter daily mean temperatures and the winter daily minimum temperatures at station n on the j^{th} day in the i^{th} year, respectively; k_i depends on the number of days of summer or winter in year i; for stage x_1, we used t_1 = 1971, and t_2 =1994; for stage x_2, t_1 = 1995, and t_2 = 2006; and for stage x_3, t_1 = 2007, and t_2 = 2015. The constant N is 518 and denotes the total number of meteorological stations used to define the wider area.

The diurnal temperature range was defined as follows:

$$D^{x_i}_s(n) = \frac{1}{t_2 - t_1 + 1}\sum_{i=t_1}^{t_2}\left(\frac{1}{k_i}\sum_{j=1}^{k_i}(T^{ij}_{s\max}(n) - T^{ij}_{s\min}(n))\right) \tag{13}$$

$$D^{x_i}_w(n) = \frac{1}{t_2 - t_1 + 1}\sum_{i=t_1}^{t_2}\left(\frac{1}{k_i}\sum_{j=1}^{k_i}(T^{ij}_{w\max}(n) - T^{ij}_{w\min}(n))\right) \tag{14}$$

where $D^{x_i}_s(n)$ and $D^{x_i}_w(n)$ represent the mean summer and winter diurnal temperature range (Section 4.3) at station n in stage x_i, respectively.

3.2.2. Precipitation

The change in precipitation can be expressed as follows:

$$\Delta_{x_2x_1}P_s(n) = P^{x_2}_s(n) - P^{x_1}_s(n) \tag{15}$$

$$\Delta_{x_2x_1}P_w(n) = P^{x_2}_w(n) - P^{x_1}_w(n) \tag{16}$$

$$P^{x_i}_s(n) = \frac{1}{t_2 - t_1}\sum_{i=t_1}^{t_2}\sum_{j=1}^{k_i} p^{ij}_s(n) \tag{17}$$

$$P^{x_i}_w(n) = \frac{1}{t_2 - t_1}\sum_{i=t_1}^{t_2}\sum_{j=1}^{k_i} p^{ij}_w(n) \tag{18}$$

where $\Delta_{x_2x_1}P_s(n)$ and $\Delta_{x_2x_1}P_w(n)$ are the changes in accumulated precipitation in summer and winter (Section 4.5) at station n from stage x_1 to stage x_2, respectively; $p^{x_i}_s(n)$ and $p^{x_i}_w(n)$ are accumulated precipitation in summer and winter at station n at stage x_i, respectively; $p^{ij}_s(n)$ and $p^{ij}_w(n)$ are the daily precipitation in summer and winter at station n on the j^{th} day in the i^{th} year, respectively.

3.2.3. Number of high and low temperature days

We determined the threshold from the 95$^{\text{th}}$ (5$^{\text{th}}$) percentile of all data in a single station and then defined a day for that station as a high (low) temperature day when the daily maximum (minimum) temperature was higher (lower) than this threshold. Since the threshold for each individual station was based on its own original climate data, the threshold combines extreme characteristics with local climatic characteristics. The threshold temperature $T_{s\max th}$ or $T_{w\min th}$ can be defined as follows:

$$h^{ij}(n) = \begin{cases} 1 & T^{ij}_{s\max}(n) \geq T_{s\max th}(n) \\ 0 & T^{ij}_{s\max}(n) < T_{s\max th}(n) \end{cases} \tag{19}$$

$$l^{ij}(n) = \begin{cases} 1 & T^{ij}_{w\min}(n) \leq T_{w\min th}(n) \\ 0 & T^{ij}_{w\min}(n) > T_{w\min th}(n) \end{cases} \tag{20}$$

$$\frac{\sum_{i=1971}^{2015}\sum_{j=1}^{y_i} h^{ij}(n)}{\sum_{i=1971}^{2015}\sum_{j=1}^{y_i} 1} = 0.05 \quad (21)$$

$$\frac{\sum_{i=1971}^{2015}\sum_{j=1}^{y_i} l^{ij}(n)}{\sum_{i=1971}^{2015}\sum_{j=1}^{y_i} 1} = 0.05 \quad (22)$$

$$H^{x_i}(n) = \frac{1}{t_2 - t_1 + 1}\sum_{i=t_1}^{t_2}\sum_{j=1}^{k_i} h^{ij}(n) \quad (23)$$

$$L^{x_i}(n) = \frac{1}{t_2 - t_1 + 1}\sum_{i=t_1}^{t_2}\sum_{j=1}^{k_i} l^{ij}(n) \quad (24)$$

where h^{ij}(n) and l^{ij}(n) represent the number of high and low temperature days, respectively; y_i depends on the number of days in year i; and H^{x_i}(n) and L^{x_i}(n) represent the frequency of high temperature days in summer and low temperature days in winter (Section 4.4) in stage x_i. In addition, the frequency of high and low temperature days in every month (months 6, 7 and 8 in summer; months 12, 1, and 2 in winter) was calculated (see Fig. 6).

3.3. Mann-Kendall test

The MK test (Mann 1945, Kendall 1975) determines the trend based on the statistic:

$$S = \sum_{i=1}^{n-1}\sum_{j=i+1}^{n} \text{sign}(x_j - x_i) \quad (25)$$

where x_i and x_j are elements of a sequential data series, with i = 1, 2, 3,...n – 1 and j = 1, 2, 3,...n – 1; n is the sample size; and

$$\text{sign}(\theta) = \begin{cases} +1 & \theta > 0 \\ 0 & 0 \\ -1 & \theta < 0 \end{cases} \quad (26)$$

When $n \geq 8$, the statistic, S, follows an approximately normal distribution with the mean and variance expressed as follows (Marengo et al. 1998, Joshi et al. 2016, Ruml et al. 2017):

$$E(S) = 0; Var(S) = \frac{n(n-1)(2n+5) - \sum_{i=1}^{n} t_i(t_i)(2t_i+5)}{18} \quad (27)$$

where t_i is the number of ties of extent i. The standardized test statistic, Z_{MK}, is expressed as follows:

$$Z_{MK} = \begin{cases} \frac{S-1}{\sqrt{Var(S)}} & S > 0 \\ 0 & S = 0 \\ \frac{S+1}{\sqrt{Var(S)}} & S < 0 \end{cases} \quad (28)$$

Under the null hypothesis, the assumption is a lack of trends; however, the null hypothesis will be rejected when the absolute value of Z_{MK} is >1.96 at a significance level of 0.05.

When the MK method is used to test the aberrance of the series, the test statistic is expressed as follows:

$$\text{UF}_k = (s_k - E(s_k)) / \sqrt{Var(s_k)} \qquad (k = 2, 3, \ldots n) \quad (29)$$

$$s_k = \sum_{i=1}^{k}\sum_{j}^{i-1} \alpha_{ij} \quad , \quad \alpha_{ij} = \begin{cases} 1 & xi > xj \\ 0 & xi < xj \end{cases} \quad 1 \leq j \leq i \quad (30)$$

$$E(s_k) = k(k+1)/4 \quad (31)$$

$$\text{Var}(s_k) = k(k-1)(2k+5)/72 \quad (32)$$

where s_k is a cumulative number, E is average, Var is variance, α is judgement, UF_k is the forward sequence, and the backward sequence, UB_k, is calculated using the same equation but with a reversed series of data. The null hypothesis (no step change point) is rejected if any of the points in the forward sequence UF_k are outside the confidence interval. A positive UF_k value denotes a positive trend and a negative value denotes a negative trend; if the value exceeds the significance level, it indicates a significant trend (Wang et al. 2012, Ye et al. 2013). The sequential MK test is often used to determine the approximate time of occurrence of a change point by locating the intersection of the forward and backward curves of the test statistic. An intersection point of UF_k and UB_k located within the confidence interval indicates the beginning of a step change point (Gerstengarbe & Werner 1999, Ye et al. 2013), which is defined as the mutation time in this paper. Generally, the confidence level was set at 0.05. We calculated the yearly average of the number of high and low temperature days in different regions, and investigated mutation times of the number of the high and low temperature days in different regions using the MK test.

3.4. EVI and LST trends

We processed the EVI and daytime LST data to determine the seasonal means and then performed a yearly linear trend analysis, and tested the signifi-

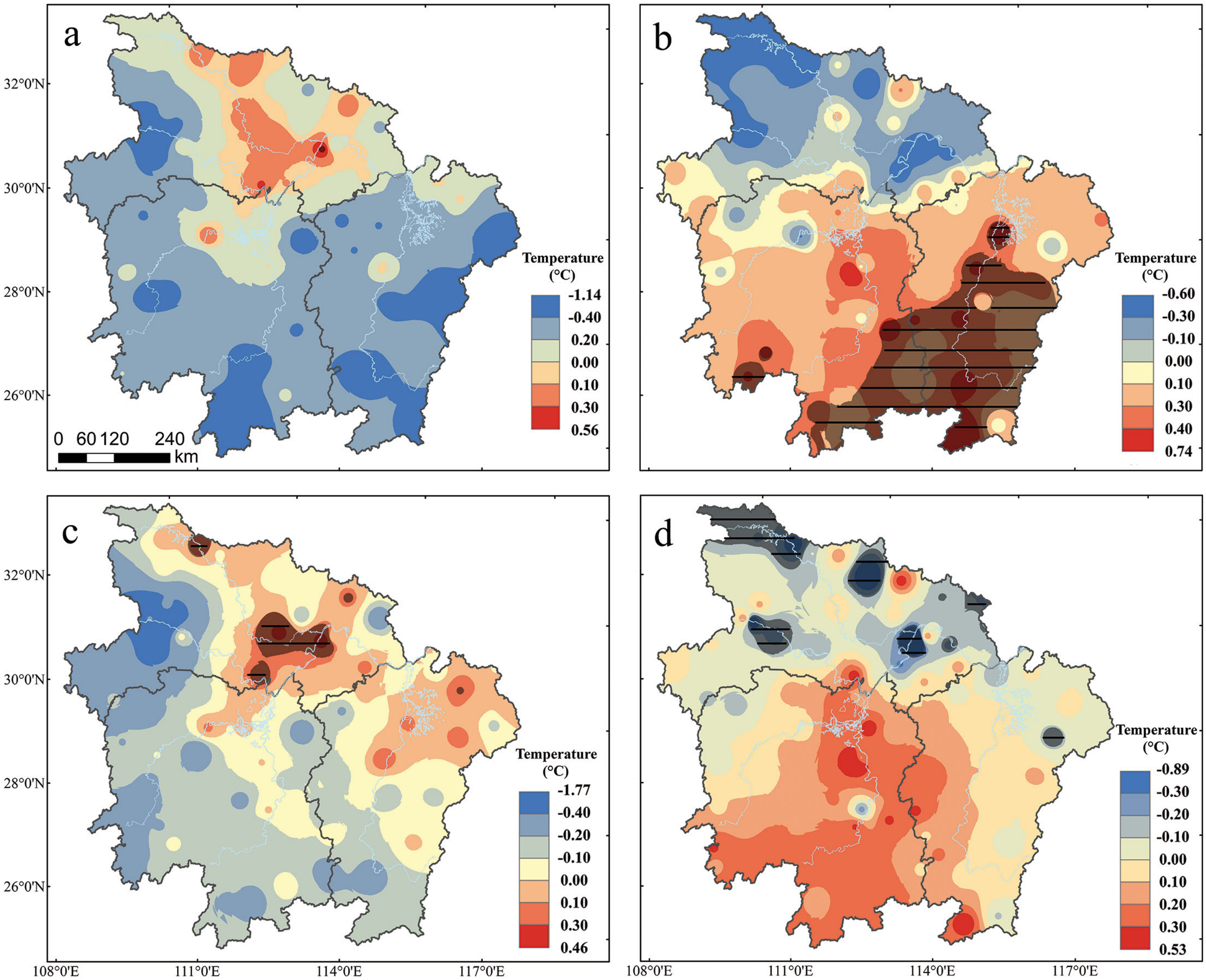

Fig. 2. Spatial distribution of changes in (a,b) summer and (c,d) winter daily mean temperature from (a,c) stage 1 to stage 2 and (b,d) stage 2 to stage 3. Dark shaded regions with horizontal lines: significant at the 95% confidence level; statistical significance was evaluated based on 2-tailed Student's *t*-tests (the same applies to Figs. 3, 4, 5 & 8)

cance of results via *t*-tests (0.05 significance level). The data were processed by geometric correction and radiometric correction. To correct for pixels that did not show data in the 8-day LST images because of cloud cover, we only took into account valid data points to calculate the seasonal means.

4. RESULTS

4.1. Daily mean temperature

We analyzed the changes in daily mean temperature during the summer season (Eq. 1) from stage 1 to stage 2 and from stage 2 to stage 3. From stage 1 to stage 2, positive values during summer occurred mostly in the northern study area, and the maximum value was 0.56°C in the Wuhan region (Fig. 2a). From stage 2 to stage 3, there were positive changes in the south and negative changes in the north with the Yangtze River as the dividing line. High negative values were distributed in the Danjiangkou region and the Wuhan region, and a minimum value of −0.60°C was observed in the Wuhan region. High positive values were distributed along the Xiangjiang River and the Ganjiang River, with a maximum value of 0.74°C observed in the southern region of Dongting Lake. Only the southeastern part of the study area showed significant changes (Fig. 2b).

Fig. 2c shows the changes in daily mean temperature during the winter season (Eq. 2) from stage 1 to stage 2. Most of the study area showed a downward trend in daily mean temperature, except the Wuhan region and the Poyang Lake region; the only significant area was in the Wuhan region. From stage 2 to stage 3, a warming zone was observed along the Xiangjiang River, and the maximum value was 0.53°C in the Dongting Lake region, whereas a cooling zone was found in the Wuhan region, and the significant areas were scattered sporadically in the northern study area. The winter daily mean temperature in the Dongting Lake region showed an upward trend, which was similar to that of the summer daily mean temperature (Fig. 2d).

4.2. Daily maximum and minimum temperature

Fig. 3a maps the changes in daily maximum temperature during the summer season (Eq. 3) from stage 1 to stage 2. Whereas the southern region showed a decrease in summer daily maximum temperature from stage 1 to 2, the northern region exhibited an increase. From stage 2 to stage 3, the pattern reversed, such that the southern study area became a warming zone, and the northern area became a cooling zone. Regions to the south of the Yangtze River experienced an increase in the summer daily maximum temperature. High positive values occurred around the lakes and rivers, and the maximum was 0.68°C in southern Jiangxi Province. Furthermore, the significant areas were mainly dis-

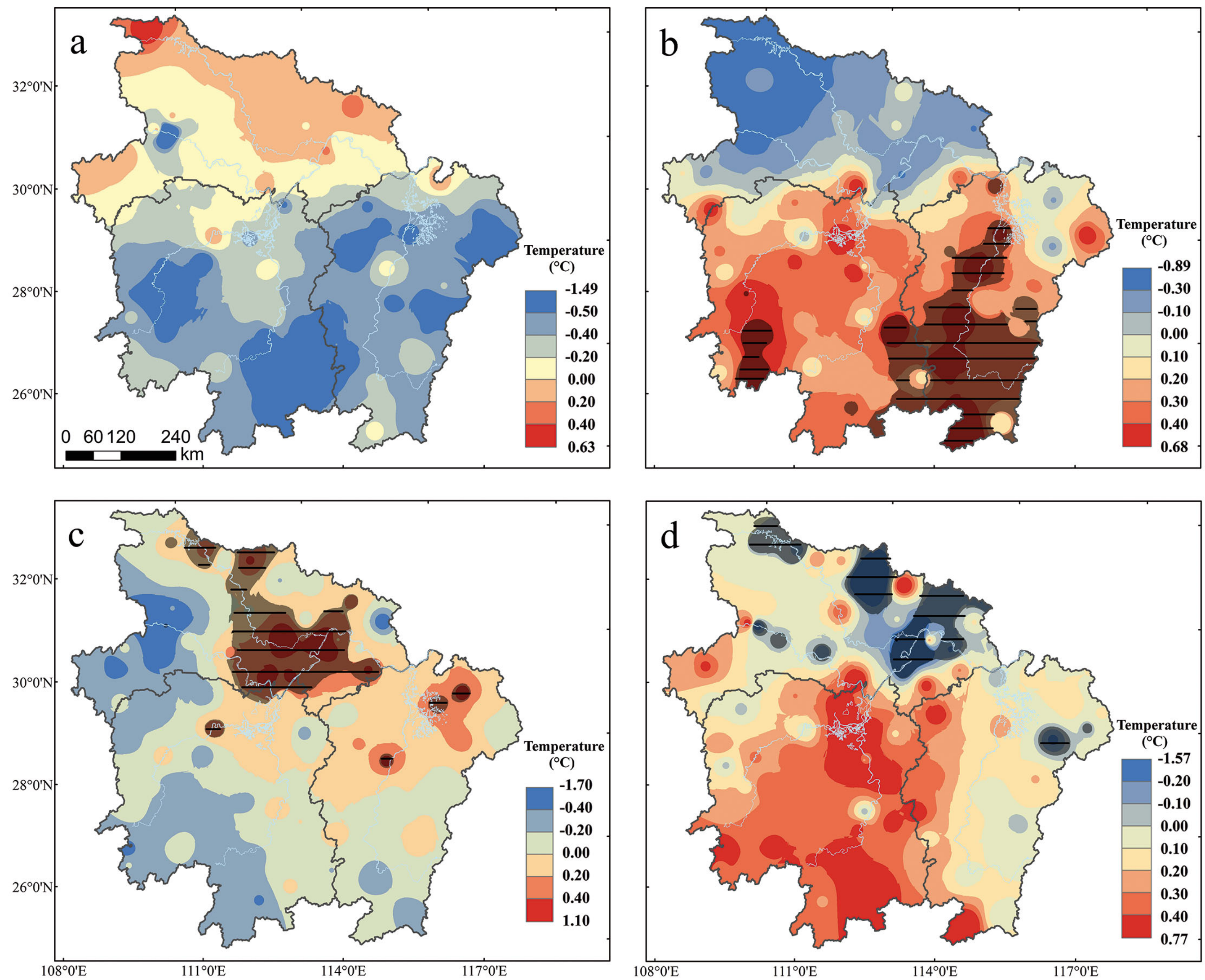

Fig. 3. Spatial distribution of changes in (a,b) summer and (c,d) winter daily maximum temperature from (a,c) stage 1 to stage 2 and (b,d) stage 2 to stage 3. Other datails as in Fig. 2

tributed along the Ganjiang River. However, the summer daily maximum temperature decreased in Hubei Province, which showed a minimum value of −0.89°C (Fig. 3b).

From stage 1 to stage 2, large positive changes occurred in daily minimum temperature during the winter season (Eq. 4) in the northeastern study area, and the maximum value of 1.10°C was observed in the Wuhan region, which showed a significant increase (Fig. 3c). Large negative changes were observed in the Three Gorges region. From stage 2 to stage 3, the Wuhan region became a significant cooling zone, and featured a minimum value of −1.57°C, whereas regions along the Xiangjiang River and the Dongting Lake were warming zones (a maximum of 0.77°C was observed in the Dongting Lake region; Fig. 3d).

4.3. Diurnal temperature range

Fig. 4a shows a downward trend in the summer diurnal temperature range (Eq. 13) from stage 1 to stage 2 distributed in the middle of the study area. Small areas mostly located in western Hubei Province had positive values. From stage 2 to stage 3, the areas that showed increased summer diurnal temperature ranges (Fig. 4b) were mostly located in the Wuhan region and the Yuanjiang River region (maximum value of 0.71°C was observed in the Wuhan region), whereas decreases were observed in the northwestern and northeastern study area, the significant areas were mainly in the middle northern study area.

Changes in the winter diurnal temperature range (Eq. 14) were observed in the middle of the study area,

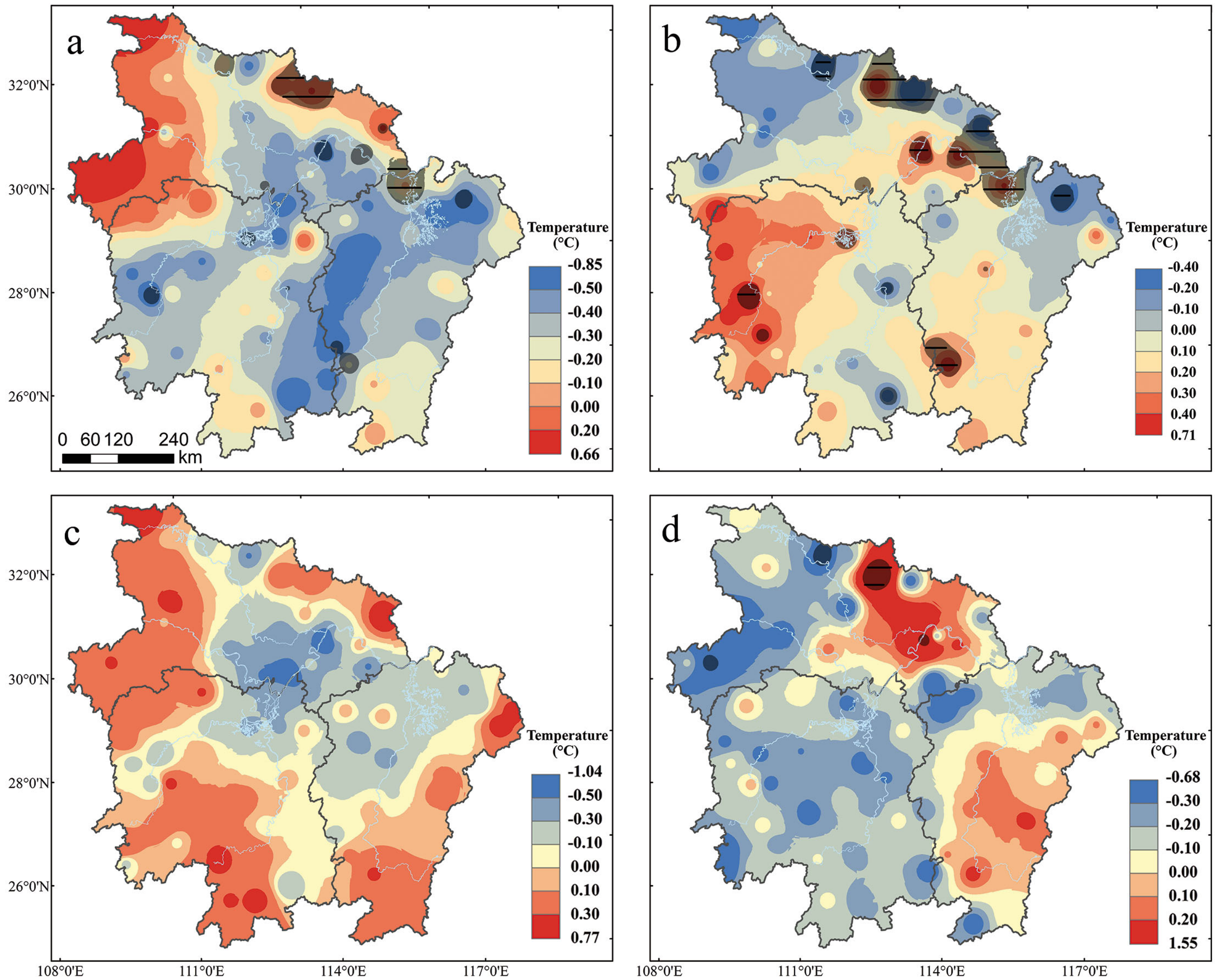

Fig. 4. Spatial distribution of changes in (a,b) summer and (c,d) winter daily maximum temperature from (a,c) stage 1 to stage 2 and (b,d) stage 2 to stage 3. Other datails as in Fig. 2

which showed negative values from stage 1 to stage 2, but there was no significant area (Fig. 4c). From stage 2 to stage 3, the Wuhan region experienced an increase in the diurnal temperature range, with a maximum value of 1.55°C. The southern and western part of our study area experienced small changes in the winter diurnal temperature range, and a minimum value of −0.68°C was observed in the southern Three Gorges region (Fig. 4d). In general, significant changes could only be found on rather local scales.

4.4. Number of high and low temperature days

Fig. 5a shows that small areas exhibited a decrease in the frequency of summer high temperature days (Eq. 23) from stage 1 to stage 2, and that these areas were in western Poyang Lake and in the Three Gorges region. High positive values were concentrated in the northern study area. From stage 2 to stage 3, the northern study area showed a downward trend in the frequency of summer high temperature days, whereas the southern study area showed an upward trend, and the significant area was located along the Ganjiang River (Fig. 5b).

The frequency of low temperature days in winter (Eq. 24) generally decreased over the whole study area from stage 1 to stage 2, and high values were concentrated in the Dongting Lake region, the Poyang Lake region and the Wuhan region; the minimum value was −14.5 d yr^{-1} (Fig. 5c). However, the change observed from stage 2 to stage 3 were com-

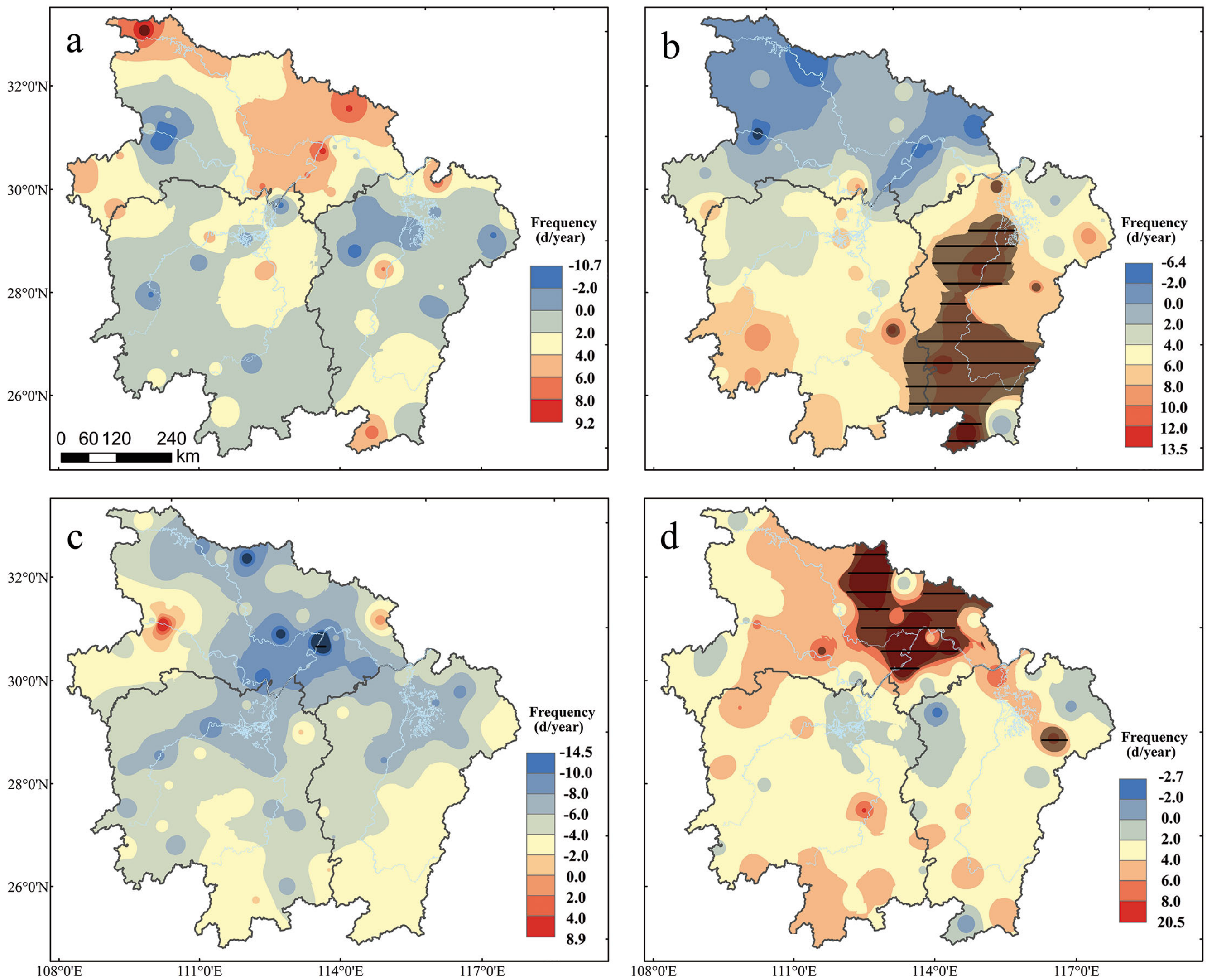

Fig. 5. Spatial distribution of changes in (a,b) summer and (c,d) winter daily maximum temperature from (a,c) stage 1 to stage 2 and (b,d) stage 2 to stage 3. Other datails as in Fig. 2

pletely different from that from stage 1 to stage 2, with the frequency of low temperature days in winter increasing in the study area. High positive values were observed in the northern study area, and the significant area was located in the Wuhan region (Fig. 5d).

According to Fig. 5, the major changes in the frequency of low temperature days were mainly concentrated in the northern study area, and the major changes in the frequency of high temperature days were mainly concentrated in the southern study area. We further studied the monthly frequencies of high temperature days in summer and low temperature days in winter for southern and northern study areas during the 3 stages. In Fig. 6, high temperature days in each summer month in the southern study area occurred more frequently in stage 3 than in the first 2 stages. The frequency of high temperature days increased from 1.1 to 2.0 d mo^{-1} in June; from 9.0 to 11.1 d mo^{-1} in July; and from 6.7 to 9.7 da mo^{-1} in August. In the northern area, the frequency of high temperature days decreased from stage 2 to stage 3 in June and July. However, the frequency of low temperature days decreased from stage 1 to stage 2 and increased from stage 2 to stage 3, except in the southern area in December, and the northern area showed a stronger increase than the southern area from stage 2 to stage 3.

Changes in the number of high and low temperature day series in the southern and northern study areas and the corresponding MK test results are shown in Fig. 7a–d. As depicted in Fig. 7a, the number of high temperature days in the southern area showed a long-term upward trend that was gradual from 1985 to 2015 and then rapid from 2004 to 2015. Fig. 7b shows that the UF values for the number of high temperature days were below zero from 1971–1977 and that they did not surpass the critical value lines. Afterwards, the UF values were was near the zero line until 2003; however, an abrupt change occurred in the variables in 2002–2003 at the 0.05 significance level, and the intersection point of the 2 curves was located within the confidence interval. An obvious increasing tendency began in 2003, and this trend was significant during the period 2010–2015 because the values of UF were above the critical limit. As shown in Fig. 7c, the number of low temperature days in the northern study area showed a downward trend from 1971–2002 and an upward trend thereafter. The UF curve intersected with the UB curve in 1984–1985 within the confidence interval (Fig. 7d), and the values of UF were below zero after 1987. The curve penetrated the critical line for the period from 1995–2009, which indicated a significant decrease. However, the UF curve increased after 2006 and then rose upward through the critical line in 2010. For the Dongting Lake region and the Poyang Lake region (Fig. 7e,i) the mutation time of high temperature days was in 2001, and a marked upward trend was observed thereafter. The number of low temperature days in these 2 regions (Fig. 7h,l) did not show the same changes observed in the northern study area, where the UF curve increased after 2006 and then rose upward through the critical line. In the Wuhan region (Fig. 7p), a more obvious tendency was observed compared with the northern area (Fig. 7d). The UF curve of the number of high temperature days in the Wuhan region (Fig. 7n) did not penetrate the critical line as in the southern study area.

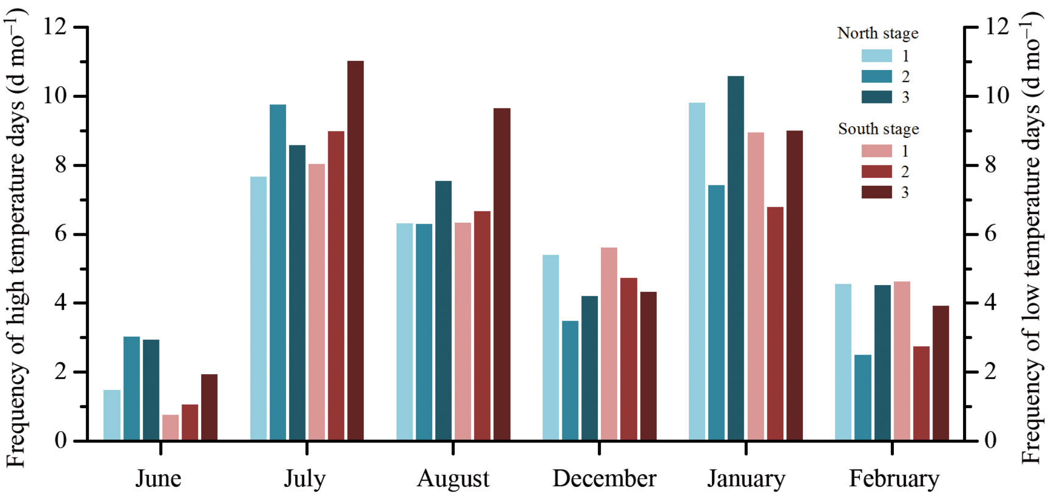

Fig. 6. Monthly frequencies of high temperature days in summer and low temperature days in winter for southern and northern study areas during the 3 stages

4.5. Precipitation

Accumulated precipitation for the entire season was calculated for both summer and winter (Eqs. 15 to 18). In summer, the precipitation levels increased in the Dongting Lake region and in most of the eastern study area from stage 1 to stage 2, with a maximum value of 21.8 mm; nevertheless, there was no significant area (Fig. 8a). Fig. 8b indicates that the precipitation decreased in the middle study area, with a minimum value of −17.6 mm from stage 2 to stage 3. Small precipitation increases were observed in certain areas, including the Three Gorges region, eastern Hubei Province and northern Jiangxi Province, and the maximum value was 7.0 mm in the Three Gorges region. The significant areas were mainly located in the Dongting Lake region.

In winter, an area with markedly enhanced precipitation from stage 1 to stage 2 was observed along the Yangtze River that stretched up to the Yuanjiang River, and a maximum value of 7.0 mm was observed in the southwestern Dongting Lake region (Fig. 8c). From stage 2 to stage 3, most of the study area showed dryer conditions. The Yuanjiang River region near Dongting Lake showed decreased precipitation, and the minimum value in the decreasing zone was −8.3 mm. The significant areas covered the Dongting lake region and the northern study area. The only zones with increasing precipitation were in the southern and northeastern regions of Jiangxi Province (Fig. 8d).

4.6. The EVI and LST

We calculated the linear trends of the EVI and LST in summer and winter from 2006–2015. The summer EVI trend in a majority of the study area (71.1%) was positive; the percentage of the area in green (Fig. 9a), which showed a significant increase, was 12.8%. The percentage of the area in purple, which showed negative values, was 28.9%, and the area with significantly negative values accounted for 3.2% (Table 1). Areas with significantly increased vegetation index values were primarily distributed in the high-elevation areas. The downward trend coefficients were concentrated in the northern study areas, mainly distributed along the Yangtze River, Dongting Lake and Poyang Lake (Fig. 9a). The summer LST increased in the northern and western study areas (50.1%). The areas with significant upward trends were concentrated in the Wuhan region, the Dongting Lake region and central Hubei Province (1.9%). LST decreased in the southeastern portion of the study areas, in the east and in western Hubei Province (49.9%), while the areas with significant decreases were mostly in the Poyang Lake region (Fig. 9b).

For the winter EVI, significant upward trends were mostly mapped in the south of the Yangtze River (34.0%), and while significant downward trends were mapped in the northern study area (1.2%), it was generally smaller than that in summer (3.2%) (Fig. 9c). Fig. 9d shows that the winter LST decreased in most of the southern study area (59.1%), and increased in the northern study area, the Dongting lake region and the Poyang lake region (40.9%). However, the significant positive and negative areas only accounted for 0.1 and 0.2%, respectively.

5. DISCUSSION

Under the background of changes in the hydrological regime after the commissioning of the TGD, we identified regional climate changes and vegetation variations in the areas downstream of the TGD. When global warming interference was eliminated, from stage 2 to stage 3 the daily mean temperature and daily maximum temperature were found to have significantly increased in the southeastern study area in summer, while the daily mean temperature and daily minimum temperature were found to have significantly decreased in the Wuhan and surrounding regions in winter. The diurnal temperature range increased in both seasons, and these changes are inconsistent with the variation observed from stage 1 to stage 2. Moreover, the frequencies of high and low temperature days showed a similar spatial distribution to that of the temperatures.

Precipitation in the middle reaches of the Yangtze River declined from stage 2 to stage 3 in summer and winter. Dongting Lake and its surrounding area was

Fig. 7. Left column: time series of the number of high or low temperature days (see *y*-axis) in summer in (a,b) the southern area, (c,d) the northern area, (e–h) the Dongting Lake region, (i–l) the Poyang Lake region and (m–p) the Wuhan region. Right column: the corresponding Mann-Kendal (MK) trend tests. Dashed lines in the left-hand figures are cubic polynomial trend lines; short dashed lines in the right-hand figures represent the critical value with a 0.05 significance level. UF and UB: forward and backward sequences, respectively

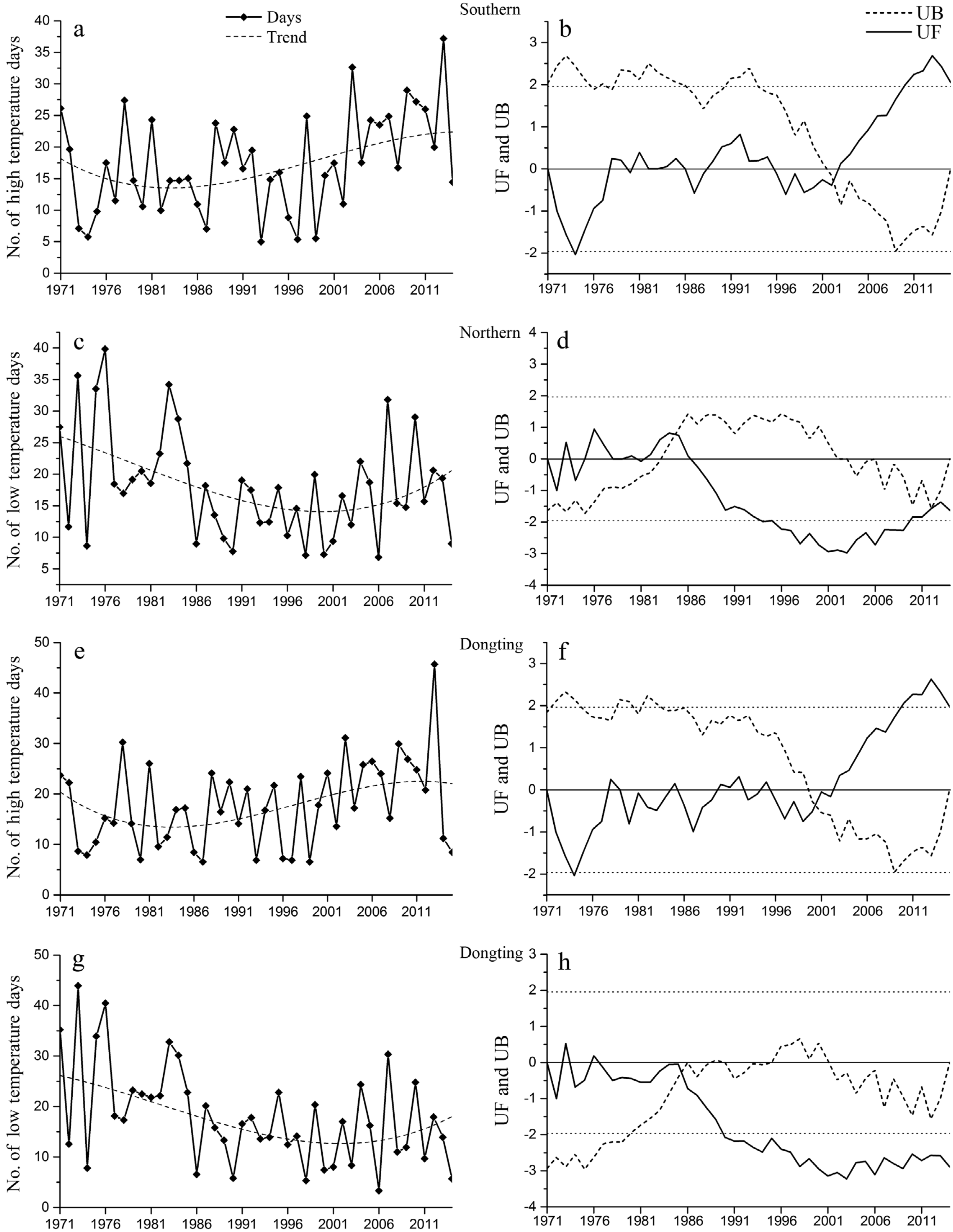
Southern
Northern
Dongting
Dongting
a
b
c
d
e
f
g
h
Days
Trend
UB
UF
No. of high temperature days
No. of low temperature days
UF and UB
1971
1976
1981
1986
1991
1996
2001
2006
2011

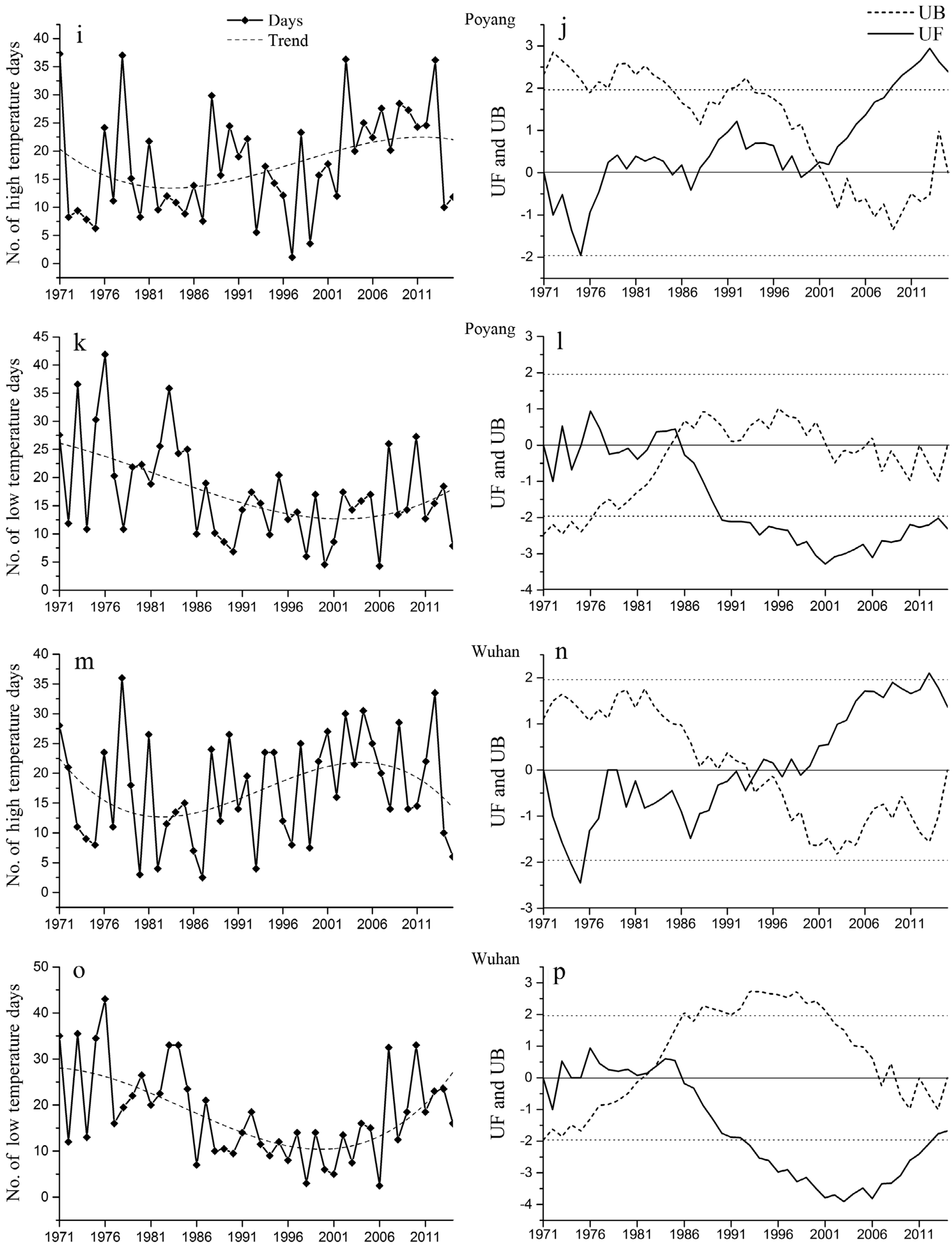

Fig. 7 (continued)

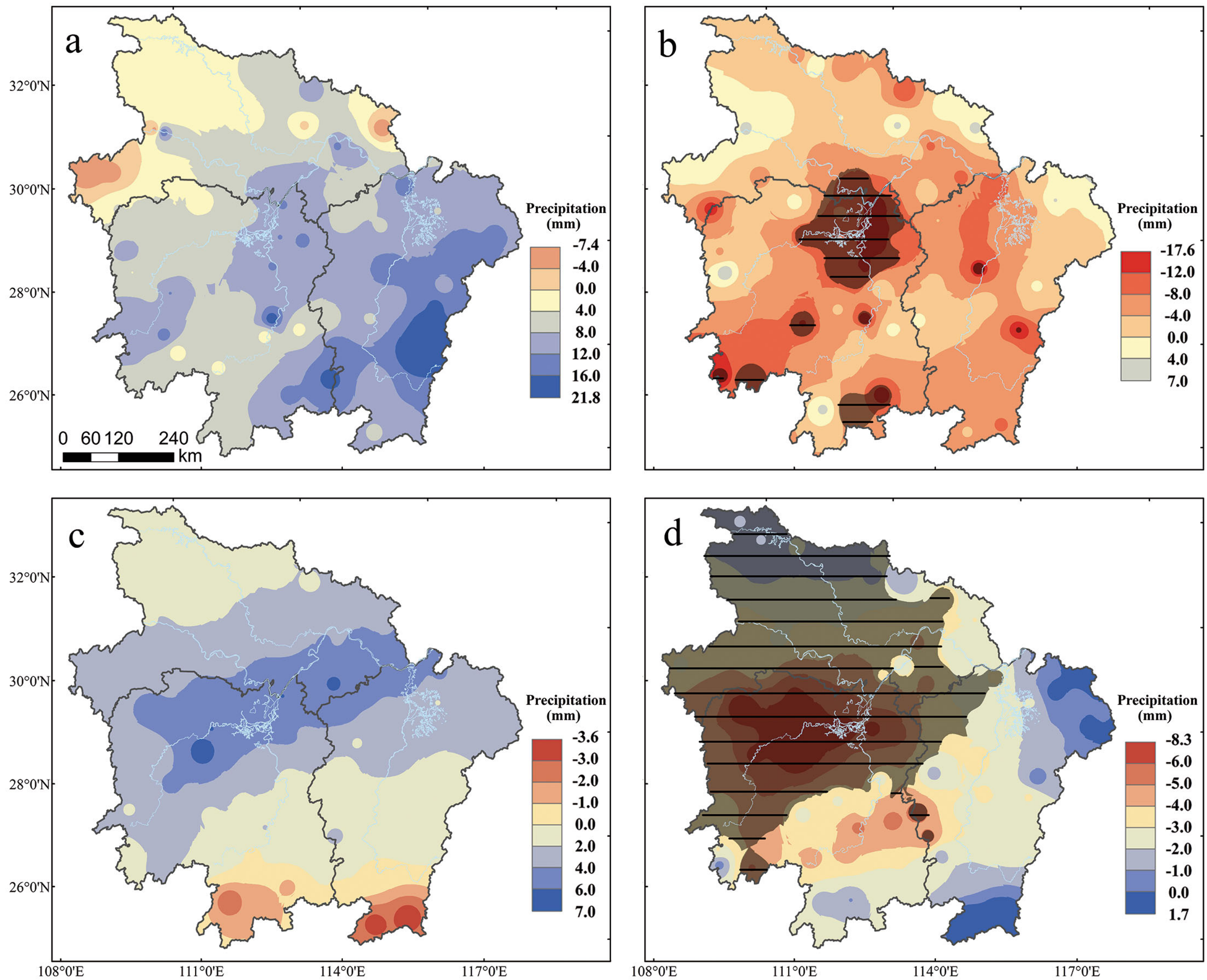

Fig. 8. Spatial distribution of changes in (a,b) summer and (c,d) winter daily maximum temperature from (a,c) stage 1 to stage 2 and (b,d) stage 2 to stage 3. Other details as in Fig. 2

the most significantly affected region. Compared with the abundant precipitation in the middle reaches of the Yangtze River (Deng et al. 2016, Tian et al. 2016), changes in precipitation levels from stage 2 to stage 3 were not sufficient to noticeably affect the discharge.

From stage 1 to stage 2, there were few areas that showed significant changes in the above factors, which means that the changes during this period can be attributed to natural variability. However, from stage 2 to stage 3, these factors showed significant changes. The MK aberrance test results also showed that the mutation times of the number of high temperature days in summer in the southern study area, including the Dongting Lake and Poyang Lake regions, and the number of low temperature days in winter in the northern study area, including the Wuhan region, occurred around the time that the TGD began commissioning. We hold the opinion that the above factors changed significantly in certain regions after commissioning of the TGD.

Temperatures generally increased in the study area after TGD commissioning began, and the trend varied from north to south. Under conditions of global warming (Jiang & Zhang 2015), vegetation showed increased coverage in most regions during summer and winter under the changed climate and hydrological regime, except in the Wuhan region, the Dongting Lake region and the Poyang Lake region. Increased vegetation coverage was more obvious in winter, while the decreased vegetation coverage was more obvious in summer. Vegetation can

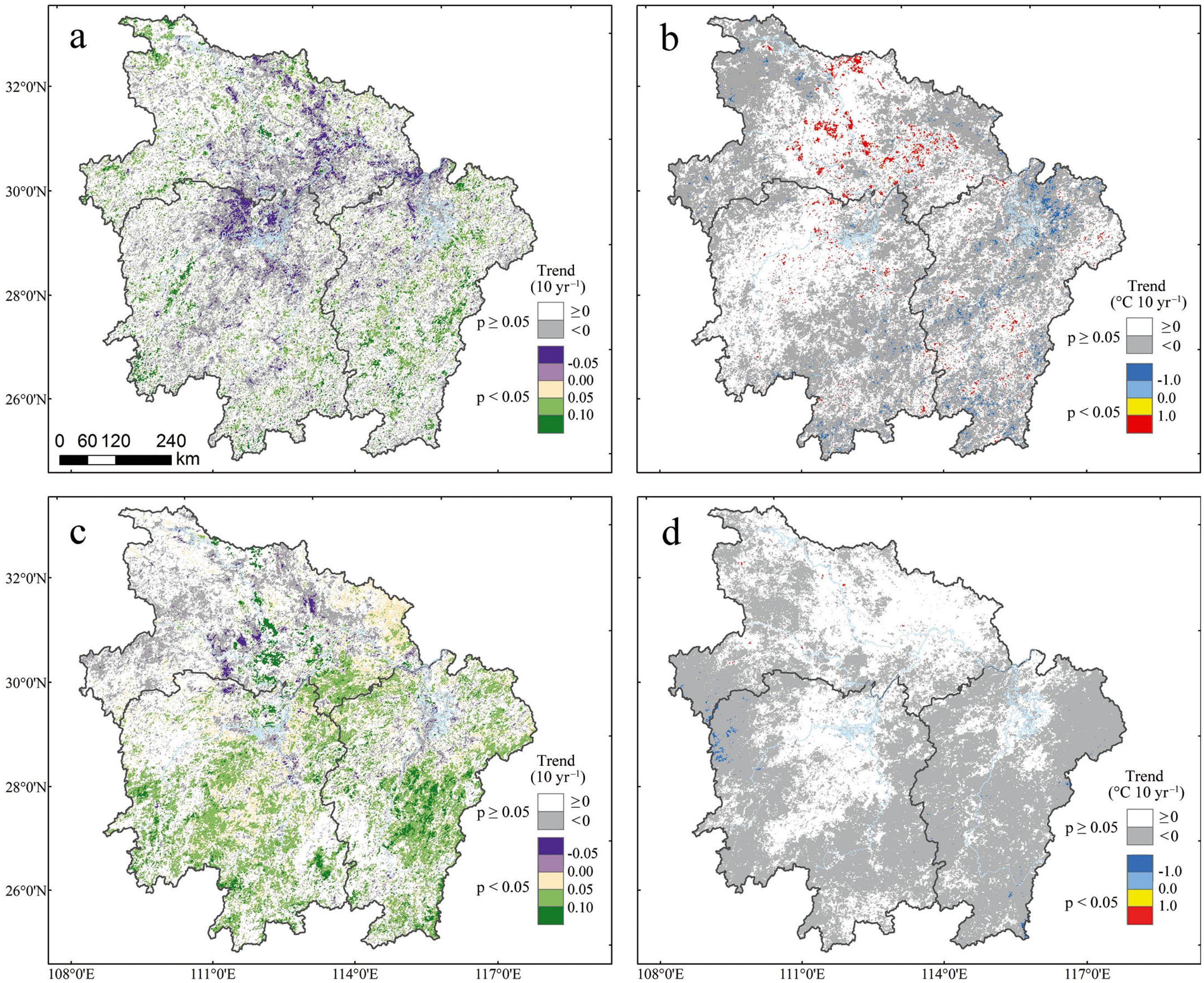

Fig. 9. Spatial distribution of (a) enhanced vegetation index (EVI) trend and (b) land surface temperature (LST) trend in summer during 2006–2015. Panels (c) and (d) are the same as (a) and (b), respectively; but for winter EVI and LST. White and gray: non-significant positive and negative EVI changes, respectively; significant EVI change is shown in the colored areas

affect the LST and the land surface energy balance by altering the exchange of energy and water between the land surface and the air (Li et al. 2009, Petropoulos et al. 2014), and the vegetation index presented triangular and trapezoidal relationships with the LST under different conditions (Moran et al. 1994, Carlson et al. 1995, Kustas et al. 2003). The LST is a vital parameter in the physics of land surface processes on regional

Table 1. Percentage of areas showing positive and negative trend values for the enhanced vegetation index (EVI) and land surface temperature (LST) during 2006–2015. Significance: $p < 0.05$

Season	EVI		LST	
Trend value	% of study area	% with significant trends	% of study area	% with significant trends
Summer				
Positive	71.1	12.8	50.1	1.9
Negative	28.9	3.2	49.9	1.1
Winter				
Positive	86.0	34.0	40.9	0.1
Negative	14.0	1.2	59.1	0.2

and global scales, and the LST values were combined with the results of all surface–atmosphere interactions and energy fluxes between the atmosphere and the ground (Wan et al. 2002, Wan 2008). Areas in this study with a significant negative EVI trend usually had a positive LST trend, particularly in the Wuhan region, the Dongting Lake region and the Poyang Lake region. In summer and winter, regions in the southern study area showed a significant positive EVI trend that was generally accompanied by a negative LST trend, and the LST decrease may have been caused by greater vegetation transpiration. In the southern study area, the summer air temperatures and high temperature days showed greater increases than those in the northern study area. The increased air temperature played a positive role in vegetation growth in the southern study area, which is generally consistent with the study by Y Zhang et al. (2014). However, high temperatures can also induce vegetation stomatal closure, which may further decrease the surface latent heat flux and increase the sensible heat flux (McDowell et al. 2008); therefore, certain regions with positive EVI trends in the southern study area also had positive LST trends. LST has a positive effect on air temperature, and the distribution of summer and winter EVI trends were similar to those of the air temperature trends in this study, likely because of the feedback between vegetation and the regional climate.

6. CONCLUSIONS

This study demonstrated that regional climate changed significantly in the middle reaches of the Yangtze River after the commissioning of the TGD, and the TGD is a possible cause. There may be different ways of taking into account the global warming background, and the influence of nonlinearities and teleconnections cannot be ruled out at this stage. Trends in the EVI changes were identified and may provide a reference for local agricultural zoning. Local climate change is also affected by other factors, such as global-scale climate variability and changes of land–sea thermal contrasts. Thus, further analysis of specific influence mechanisms is warranted, and additional attention should be focused on projects that involve regional economic and ecological systems.

Acknowledgements. The authors thank the Goddard Space Flight Center for providing the MODIS data, and Dr. Tony from the University of Toronto for improving the English. This work was supported by the National Key R&D Program of China (2016YFC0500203), National Natural Science Foundation of China (No.41571427), and Innovative Group Guide Project (Grant No. Y2017JC33), and Open Fund of State Key Laboratory of Remote Sensing Science (Grant No. OFSLRSS201708).

LITERATURE CITED

Bossa A, Diekkrüger B, Agbossou E (2014) Scenario-based impacts of land use and climate change on land and water degradation from the meso to regional scale. Water 6:3152–3181

Cai X, Feng L, Hou X, Chen X (2016) Remote sensing of the water storage dynamics of large lakes and reservoirs in the Yangtze River Basin from 2000 to 2014. Sci Rep 6: 36405

Cao Q, Yu D, Georgescu M, Han Z, Wu J (2015) Impacts of land use and land cover change on regional climate: a case study in the agro-pastoral transitional zone of China. Environ Res Lett 10:124025

Carlson TN, Capehart WJ, Gillies RR (1995) A new look at the simplified method for remote-sensing of daily evapotranspiration. Remote Sens Environ 54:161–167

Chacón A, Sushama L, Beltrami H (2016) Biophysical impacts of land use change over North America as simulated by the Canadian regional climate model. Atmosphere (Toronto) 7:34

Chai C, Yu Z, Shen Z, Song X, Cao X, Yao Y (2009) Nutrient characteristics in the Yangtze River Estuary and the adjacent East China Sea before and after impoundment of the Three Gorges Dam. Sci Total Environ 407:4687–4695

Chen J, Wu X, Finlayson BL, Webber M, Wei T, Li M, Chen Z (2014) Variability and trend in the hydrology of the Yangtze River, China: annual precipitation and runoff. J Hydrol 513:403–412

Chen J, Finlayson BL, Wei T, Sun Q, Webber M, Li M, Chen Z (2016) Changes in monthly flows in the Yangtze River, China – with special reference to the Three Gorges Dam. J Hydrol 536:293–301

Chen SB, Liao CS, Li ZJ, Zhang TL, Ye SW, Liu JS (2016) Length-weight relationships of 55 fish species from the Three Gorges Reservoir in the Yangtze River, China. J Appl Ichthyology 32:1268–1272

Congjian S, Yaning C, Weihong L, Xingong L, Yuhui Y (2016) Isotopic time series partitioning of streamflow components under regional climate change in the Urumqi River, northwest China. Hydrol Sci J 61:1443–1459

Dai Z, Fagherazzi S, Mei X, Gao J (2016) Decline in suspended sediment concentration delivered by the Changjiang (Yangtze) River into the East China Sea between 1956 and 2013. Geomorphology 268:123–132

Deng K, Yang S, Lian E, Li C, Yang C, Wei H (2016) Three Gorges Dam alters the Changjiang (Yangtze) river water cycle in the dry seasons: evidence from H-O isotopes. Sci Total Environ 562:89–97

Du Y, Xue H, Wu S, Ling F, Xiao F, Wei X (2011) Lake area changes in the middle Yangtze region of China over the 20th century. J Environ Manage 92:1248–1255

Du J, Yang S, Feng H (2016) Recent human impacts on the morphological evolution of the Yangtze River delta foreland: a review and new perspectives. Estuar Coast Shelf Sci 181:160–169

Fay PA, Guntenspergen GR, Olker JH, Johnson WC (2016)

Climate change impacts on freshwater wetland hydrology and vegetation cover cycling along a regional aridity gradient. Ecosphere 7:e01504

Feng L, Hu C, Chen X, Zhao X (2013) Dramatic inundation changes of China's two largest freshwater lakes linked to the Three Gorges Dam. Environ Sci Technol 47: 9628–9634

Gao X, Huete AR, Ni WG, Miura T (2000) Optical-biophysical relationships of vegetation spectra without background contamination. Remote Sens Environ 74:609–620

Gao Y, Markkanen T, Backman L, Henttonen HM, Pietikäinen JP, Mäkelä HM, Laaksonen A (2014) Biogeophysical impacts of peatland forestation on regional climate changes in Finland. Biogeosciences 11:7251–7267

Gerstengarbe FW, Werner PC (1999) Estimation of the beginning and end of recurrent events within a climate regime. Clim Res 11:97–107

Guo H, Hu Q, Zhang Q, Feng S (2012) Effects of the Three Gorges Dam on Yangtze River flow and river interaction with Poyang Lake, China: 2003-2008. J Hydrol 416-417: 19–27

Halder S, Saha SK, Dirmeyer PA, Chase TN, Goswami BN (2016) Investigating the impact of land-use land-cover change on Indian summer monsoon daily rainfall and temperature during 1951–2005 using a regional climate model. Hydrol Earth Syst Sci 20:1765–1784

Han J, Huang G, Zhang H, Li Z, Li Y (2014) Heterogeneous precipitation and streamflow trends in the Xiangxi River watershed, 1961–2010. J Hydrol Eng 19:1247–1258

Huete A, Didan K, Miura T, Rodriguez EP, Gao X (2002) Overview of the radiometric and biophysical performance of the MODIS vegetation indices. Remote Sens Environ 83:195–213

Jiang C, Zhang L (2015) Climate change and its impact on the eco-environment of the Three-Rivers Headwater Region on the Tibetan Plateau, China. Int J Environ Res Public Health 12:12057–12081

Jiang L, Ban X, Wang X, Cai X (2014) Assessment of hydrologic alterations caused by the Three Gorges Dam in the middle and lower reaches of Yangtze River, China. Water 6:1419–1434

Jiao M, Song L, Wang J, Ke Y and others (2013) Addressing the potential climate effects of China's Three Gorges Project. Bull World Meteorol Org 62(Spec Issue):49–53

Joshi N, Gupta D, Suryavanshi S, Adamowski J, Madramootoo CA (2016) Analysis of trends and dominant periodicities in drought variables in India: a wavelet transform based approach. Atmos Res 182:200–220

Justice CO, Vermote E, Townshend J, Defries R and others (1998) The Moderate Resolution Imaging Spectroradiometer (MODIS): land remote sensing for global change research. IEEE Trans Geosci Remote Sens 36:1228–1249

Kendall MG (1975) Rank correlation methods. Charles Griffin, London

Kim H, Kim Y, Song S, Lee HW (2016) Impact of future urban growth on regional climate changes in the Seoul Metropolitan Area, Korea. Sci Total Environ 571:355–363

Kim S, Noh H, Jung J, Jun H, Kim H (2016) Assessment of the impacts of global climate change and regional water projects on streamflow characteristics in the Geum River Basin in Korea. Water 8:91

Kustas WP, Norman JM, Anderson MC, French AN (2003) Estimating subpixel surface temperatures and energy fluxes from the vegetation index-radiometric temperature relationship. Remote Sens Environ 85:429–440

Li G, Zhang F, Jing Y, Liu Y, Sun G (2017) Response of evapotranspiration to changes in land use and land cover and climate in China during 2001-2013. Sci Total Environ 596-597:256–265

Li J, Wang X, Wang X, Ma W, Zhang H (2009) Remote sensing evaluation of urban heat island and its spatial pattern of the Shanghai metropolitan area, China. Ecol Complex 6:413–420

Li J, Xia Z, Wang Y (2013) Impact of the Three Gorges and Gezhouba reservoirs on ecohydrological conditions for sturgeon in the Yangtze River, China. J Hydrol Eng 18: 1563–1570

Li Q, Yu M, Lu G, Cai T, Bai X, Xia Z (2011) Impacts of the Gezhouba and Three Gorges reservoirs on the sediment regime in the Yangtze River, China. J Hydrol 403: 224–233

Li M, Duan Z, Gao X, Cao W, Liu H (2016) Impact of the Three Gorges Dam on reproduction of four major Chinese carps species in the middle reaches of the Changjiang River. Chin J Oceanology Limnol 34:885–893

Liu JP, Xu KH, Li AC, Milliman JD, Velozzi DM, Xiao SB, Yang ZS (2007) Flux and fate of Yangtze River sediment delivered to the East China Sea. Geomorphology 85: 208–224

Liu Y, Wu G, Guo R, Wan R (2016) Changing landscapes by damming: the Three Gorges Dam causes downstream lake shrinkage and severe droughts. Landsc Ecol 31: 1883–1890

Ma Y, Qin Y, Zheng B, Zhao Y and others (2016) Three Gorges Reservoir: metal pollution in surface water and suspended particulate matter on different reservoir operation periods. Environ Earth Sci 75:1413

Mann HB (1945) Nonparametric tests against trend. Econometrica 13:245–259

Marengo JA, Tomasella J, Uvo CR (1998) Trends in streamflow and rainfall in tropical South America: Amazonia, eastern Brazil, and northwestern Peru. J Geophys Res D Atmospheres 103:1775–1783

McDowell N, Pockman WT, Allen CD, Breshears DD and others (2008) Mechanisms of plant survival and mortality during drought: Why do some plants survive while others succumb to drought? New Phytol 178:719–739

Mei X, Dai Z, Fagherazzi S, Chen J (2016) Dramatic variations in emergent wetland area in China's largest freshwater lake, Poyang Lake. Adv Water Resour 96:1–10

Moran MS, Clarke TR, Inoue Y, Vidal A (1994) Estimating crop water deficit using the relation between surface-air temperature and spectral vegetation index. Remote Sens Environ 49:246–263

Müller B, Berg M, Yao ZP, Zhang XF, Wang D, Pfluger A (2008) How polluted is the Yangtze river? Water quality downstream from the Three Gorges Dam. Sci Total Environ 402:232–247

Nakayama T, Shankman D (2013a) Impact of the Three-Gorges Dam and water transfer project on Changjiang floods. Global Planet Change 100:38–50

Nakayama T, Shankman D (2013b) Evaluation of uneven water resource and relation between anthropogenic water withdrawal and ecosystem degradation in Changjiang and Yellow River basins. Hydrol Processes 27:3350–3362

Naz BS, Kao S, Ashfaq M, Rastogi D, Mei R, Bowling LC (2016) Regional hydrologic response to climate change in the conterminous United States using high-resolution hydroclimate simulations. Global Planet Change 143: 100–117

Nilsson C, Reidy CA, Dynesius M, Revenga C (2005) Fragmentation and flow regulation of the world's large river systems. Science 308:405–408
Pegg MA, Pierce CL, Roy A (2003) Hydrological alteration along the Missouri River Basin: a time series approach. Aquat Sci 65:63–72
Petropoulos GP, Griffiths HM, Kalivas DP (2014) Quantifying spatial and temporal vegetation recovery dynamics following a wildfire event in a Mediterranean landscape using EO data and GIS. Appl Geogr 50:120–131
Qin J, Liu Y, Chang Y, Liu S, Pu H, Zhou J (2016) Regional runoff variation and its response to climate change and human activities in northwest China. Environ Earth Sci 75:1366
Ruml M, Gregori E, Vujadinovi M, Radovanovi S and others (2017) Observed changes of temperature extremes in Serbia over the period 1961–2010. Atmos Res 183:26–41
Stagl J, Hattermann F (2015) Impacts of climate change on the hydrological regime of the Danube River and its tributaries using an ensemble of climate scenarios. Water 7:6139–6172
Sylla MB, Pal JS, Wang GL, Lawrence PJ (2016) Impact of land cover characterization on regional climate modeling over West Africa. Clim Dyn 46:637–650
Syvitski JPM, Vörösmarty CJ, Kettner AJ, Green P (2005) Impact of humans on the flux of terrestrial sediment to the global coastal ocean. Science 308:376–380
Tian Q, Prange M, Merkel U (2016) Precipitation and temperature changes in the major Chinese river basins during 1957-2013 and links to sea surface temperature. J Hydrol (Amst) 536:208–221
Toure A, Diekkrüger B, Mariko A (2016) Impact of climate change on groundwater resources in the Klela Basin, Southern Mali. Hydrology 3:17
Wan ZM (2008) New refinements and validation of the MODIS land-surface temperature/emissivity products. Remote Sens Environ 112:59–74
Wan ZM, Zhang YL, Zhang QC, Li ZL (2002) Validation of the land-surface temperature products retrieved from Terra Moderate Resolution Imaging Spectroradiometer data. Remote Sens Environ 83:163–180
Wang G, Zhang J, Yang Q (2016) Attribution of runoff change for the Xinshui River catchment on the Loess Plateau of China in a changing environment. Water 8:267
Wang H, Zhang M, Zhu H, Dang X, Yang Z, Yin L (2012) Hydro-climatic trends in the last 50 years in the lower reach of the Shiyang River Basin, NW China. Catena 95: 33–41
Wang Y, Rhoads BL, Wang D (2016) Assessment of the flow regime alterations in the middle reach of the Yangtze River associated with dam construction: potential ecological implications. Hydrol Processes 30:3949–3966
Woldemichael AT, Hossain F, Pielke R Sr (2014) Evaluation of surface properties and atmospheric disturbances caused by post-dam alterations of land use/land cover. Hydrol Earth Syst Sci 18:3711–3732
Wu H, Zeng G, Liang J, Zhang J and others (2013) Changes of soil microbial biomass and bacterial community structure in Dongting Lake: impacts of 50 000 dams of Yangtze River. Ecol Eng 57:72–78
Wu L, Zhang Q, Jiang Z (2006) Three Gorges Dam affects regional precipitation. Geophys Res Lett 33:L13806
Xiao X, Zhang Q, Braswell B, Urbanski S and others (2004) Modeling gross primary production of temperate deciduous broadleaf forest using satellite images and climate data. Remote Sens Environ 91:256–270
Xu K, Milliman JD (2009) Seasonal variations of sediment discharge from the Yangtze River before and after impoundment of the Three Gorges Dam. Geomorphology 104:276–283
Yang SL, Zhao QY, Belkin IM (2002) Temporal variation in the sediment load of the Yangtze river and the influences of human activities. J Hydrol 263:56–71
Yang SL, Zhang J, Xu XJ (2007) Influence of the Three Gorges Dam on downstream delivery of sediment and its environmental implications, Yangtze River. Geophys Res Lett 34:L10401
Yang SL, Milliman JD, Li P, Xu K (2011) 50,000 dams later: erosion of the Yangtze River and its delta. Global Planet Change 75:14–20
Yang SL, Milliman JD, Xu KH, Deng B, Zhang XY, Luo XX (2014) Downstream sedimentary and geomorphic impacts of the Three Gorges Dam on the Yangtze River. Earth Sci Rev 138:469–486
Yang T, Zhang Q, Chen YD, Tao X, Xu C, Chen X (2008) A spatial assessment of hydrologic alteration caused by dam construction in the middle and lower Yellow River, China. Hydrol Processes 22:3829–3843
Yang Z, Wang H, Saito Y, Milliman JD, Xu K, Qiao S, Shi G (2006) Dam impacts on the Changjiang (Yangtze) River sediment discharge to the sea: the past 55 years and after the Three Gorges Dam. Water Resour Res 42:501–517
Yao Y, Ruan L, Li H, Zhou W, Yang D, Yu J (2013) Changes of meteorological parameters and lightning current during water impounded in Three Gorges area. Atmos Res 134:150–160
Ye C, Cheng X, Zhang Y, Wang Z, Zhang Q (2012) Soil nitrogen dynamics following short-term revegetation in the water level fluctuation zone of the Three Gorges Reservoir, China. Ecol Eng 38:37–44
Ye X, Zhang Q, Liu J, Li X, Xu C (2013) Distinguishing the relative impacts of climate change and human activities on variation of streamflow in the Poyang Lake catchment, China. J Hydrol (Amst) 494:83–95
Yuan Y, Zeng G, Liang J, Huang L and others (2015) Variation of water level in Dongting Lake over a 50-year period: implications for the impacts of anthropogenic and climatic factors. J Hydrol 525:450–456
Zeng G, Chen M, Zeng Z (2013) Risks of neonicotinoid pesticides. Science 340:1403
Zhang Q, Ye X, Werner AD, Li Y, Yao J, Li X, Xu C (2014) An investigation of enhanced recessions in Poyang Lake: comparison of Yangtze River and local catchment impacts. J Hydrol 517:425–434
Zhang Y, Song C, Zhang K, Cheng X, Zhang Q (2014) Spatial-temporal variability of terrestrial vegetation productivity in the Yangtze River Basin during 2000–2009. J Plant Ecol 7:10–23
Zhou Y, Jeppesen E, Li J, Zhang Y, Zhang X, Li X (2016) Impacts of Three Gorges Reservoir on the sedimentation regimes in the downstream-linked two largest Chinese freshwater lakes. Sci Rep 6:35396

Editorial responsibility: Eduardo Zorita, Geesthacht, Germany

Submitted: March 9, 2017; Accepted: November 27, 2017
Proofs received from author(s): March 15, 2018